Current Biology *18*, 1333–1337, September 9, 2008 DOI 10.1016/j.cub.2008.07.086

Report

The *C. elegans* Zonula Occludens Ortholog Cooperates with the Cadherin Complex to Recruit Actin during Morphogenesis

Christina Lockwood,[1,3] Ronen Zaidel-Bar,[2] and Jeff Hardin[1,2,*]
[1]Program in Cellular and Molecular Biology
[2]Department of Zoology
University of Wisconsin-Madison
1117 W. Johnson Street
Madison, WI 53706

Summary

The dramatic cell-shape changes necessary to form a multicellular organism require cell-cell junctions to be both pliable and strong. The zonula occludens (ZO) subfamily of membrane-associated guanylate kinases (MAGUKs) are scaffolding molecules thought to regulate cell-cell adhesion [1–3], but there is little known about their roles in vivo. To elucidate the functional role of ZO proteins in a living embryo, we have characterized the sole *C. elegans* ZO family member, ZOO-1. ZOO-1 localizes with the cadherin-catenin complex during development, and its junctional recruitment requires the transmembrane proteins HMR-1/E-cadherin and VAB-9/claudin, but surprisingly, not HMP-1/α-catenin or HMP-2/β-catenin. *zoo-1* knockdown results in lethality during elongation, resulting in the rupture of epidermal cell-cell junctions under stress and failure of epidermal sheet sealing at the ventral midline. Consistent with a role in recruiting actin to the junction in parallel to the cadherin-catenin complex, *zoo-1* loss of function reduces the dynamic recruitment of actin to junctions and enhances the severity of actin filament defects in hypomorphic alleles of *hmp-1* and *hmp-2*. These results show that ZOO-1 cooperates with the cadherin-catenin complex to dynamically regulate strong junctional anchorage to the actin cytoskeleton during morphogenesis.

Results and Discussion

ZOO-1, the Sole Zonula Occludens Ortholog in *C. elegans*, Localizes to Junctions during Morphogenesis

The *C. elegans* genome contains a single predicted ortholog of the zonula occludens protein family, ORF Y105E8A.26, which we have named *zoo-1*, for zonula occludens ortholog (Figure S1 available online). We assayed ZOO-1 expression via immunostaining (Figure 1; Figure S2); a *zoo-1::gfp* construct shows identical localization (Movie S1). During morphogenesis, ZOO-1 becomes enriched at the borders of epidermal cells (Figure 1A; Figures S2D–S2F); elongating embryos exhibit the strongest junctional accumulation (Figures S2G and S2H). ZOO-1 is also expressed in myoblasts and persists in mature muscle cells (Figure S2G). In contrast, *zoo-1::gfp* driven by an epithelial promoter shows no muscle-associated signal (data not shown); thus muscle-associated ZOO-1 signal is due to expression specifically in muscle.

In cultured epithelial cells, ZO-1 initially associates with the adherens junction (AJ) and segregates apically to the tight junction as cells mature [4–7]. The apical junction in epidermal cells of *C. elegans* has two subdomains with distinct multiprotein complexes, the cadherin-catenin and DLG-AJM complexes [8], which can be partially resolved via light microscopy in embryos [9]. Quantitative colocalization analysis shows a high degree of overlap between ZOO-1, HMP-1/α-catenin, and JAC-1/p120 catenin but not between ZOO-1 and the DLG-1/AJM-1 complex (Figure S3).

ZOO-1 Recruitment to Junctions Is Dependent on HMR-1/Cadherin and VAB-9/BCMP1 but Independent of HMP-1/α-Catenin and HMP-2/β-Catenin

We next examined molecular requirements for ZOO-1 recruitment. Unlike AJM-1, which depends on DLG-1/Discs large for localization, ZOO-1 localizes properly in *dlg-1(RNAi)* embryos (Figures 1D–1F). Previous work in tissue culture has suggested that localization of vertebrate ZO-1 to the AJ may depend on α-catenin [10, 11]. We tested this in vivo by immunostaining *hmp-1(zu278)* null embryos for ZOO-1. However, ZOO-1 junctional localization appears largely unaffected in *hmp-1* zygotic null (data not shown) embryos, as it does in *hmp-1(RNAi)* (Figures 1G–1I) or *hmp-2/β-catenin (RNAi)* embryos (data not shown), in which both maternal and zygotic mRNA are removed [12, 13]. In contrast, *hmr-1/E-cadherin (RNAi)* completely disrupts epidermal ZOO-1 localization (Figures 1J–1L), although localization in muscle is unaffected. VAB-9/BCMP1 also localizes to the cadherin-catenin complex in epidermal cells in *C. elegans* [9]; ZOO-1 expression in *vab-9(ju6)* mutants is very similar to that in *hmr-1(RNAi)* embryos (Figures 1M–1O). These results suggest that both HMR-1 and VAB-9 are essential for recruiting ZOO-1 to the apical junction, but that they act upstream of HMP-2 and HMP-1.

Vertebrate ZO proteins directly interact with multiple claudin family members [14, 15]. However, we could detect no effects on junctional recruitment of ZOO-1 in *clc-1/2* single or double RNAi embryos nor epithelial permeability defects in *zoo-1* loss-of-function embryos in a standard assay [16] (data not shown). These data suggest that ZOO-1 is not an essential component of the paracellular permeability pathway in *C. elegans*.

zoo-1 Knockdown Results in Morphogenesis Defects

To examine consequences of loss of *zoo-1* function, we analyzed two *zoo-1* mutants, but both result in incomplete loss of *zoo-1* gene function (Supplemental Results). In order to achieve more complete *zoo-1* loss of function, we performed RNAi in an RNAi hypersensitive background (*rrf-3(pk1426)*; [17]). *zoo-1(RNAi);rrf-3* embryos have no detectable ZOO-1 expression as assessed via immunostaining (Figure S4), and knockdown can be achieved via multiple different RNAs that target *zoo-1* (data not shown). *rrf-3(pk1426)* homozygotes exhibit low levels of embryonic lethality (11.4% ± 6.3%, mean ± SD, n = 272) prior to the initiation of epidermal

*Correspondence: jdhardin@wisc.edu
[3]Present address: Department of Pathology & Immunology, Washington University School of Medicine, 660 S Euclid, Campus Box 8118, St. Louis, MO 63110

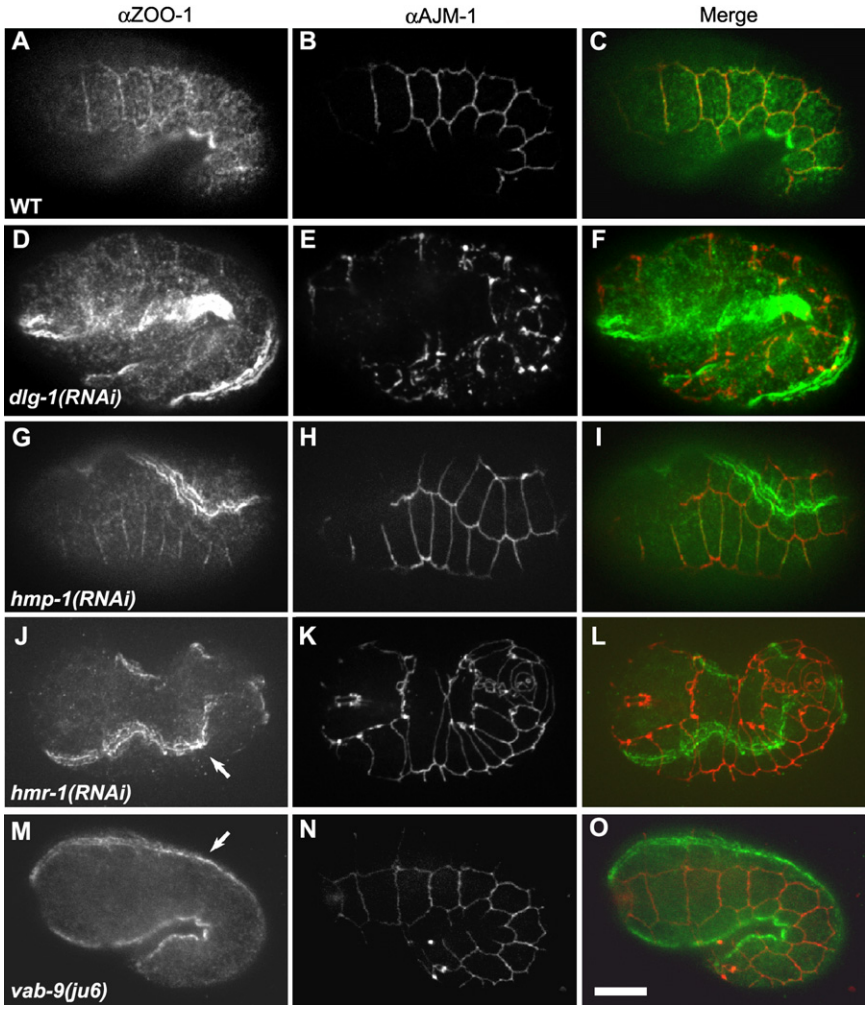

Figure 1. ZOO-1 Junctional Recruitment Is Dependent on HMR-1/E-Cadherin and VAB-9/Claudin, but Not on HMP-2/β-Catenin or HMP-1/α-Catenin

(A–L) Confocal images of elongating embryos stained for ZOO-1 (green in [A], [D], [G], [J], [M]), AJM-1 as a junctional marker (red in [B], [E], [H], [K], [N]), and the merged image (C, F, I, L, O). Wild-type (A–C), *dlg-1(RNAi)* (D–F), and *hmp-1(RNAi)* (G–I) embryos display proper junctional localization of ZOO-1, despite disruption of AJM-1 localization in the case of dlg-1(RNAi) (E). (J–L) *hmr-1(RNAi)* embryo exhibits abrogated junctional ZOO-1 staining, though staining persists in sarcomeres (J, arrow).

(M–O) *vab-9(ju6)* embryo lacks junctional ZOO-1 staining, though ZOO-1 localization in sarcomeres in unaffected ([M], arrow).

Scale bar represents 10 μm.

morphogenesis, because of gastrulation failure (data not shown). Although the penetrance of gastrulation defects in double mutants is similar to *rrf-3* single mutants, *zoo-1(RNAi)* in an *rrf-3(pk1426)* background increased overall lethality to 33.2% ± 5.9% (n = 247) and yielded multiple morphogenetic defects (Figure 2). *zoo-1(RNAi);rrf-3* embryos (Figures 2G–2I) properly complete ventral enclosure and initiate elongation; however, the rate of elongation is markedly slower than in wild-type (Figures 2A–2C; Movie S2) or *rrf-3* (Figures 2D–2F; Movie S3) animals, and abnormal bulges develop along the body (Figure 2I). Body wall muscle is functional in arrested *zoo-1;rrf-3* embryos, which continue to twitch, and muscle morphology appears normal via phalloidin staining (Figure S4H), suggesting that these defects are epidermal in nature. 6% of *zoo-1(RNAi);rrf-3* embryos exhibit epidermal rupture during elongation (Figures 2J–2L; Movie S4). The distribution and dynamics of HMP-1::GFP and JAC-1::GFP are normal in living *zoo-1(RNAi);rrf-3* embryos, and we could not detect enhancement of morphogenetic defects after ZOO-1 depletion in *vab-9(ju6)* null mutants (data not shown). The simplest interpretation of these results is that ZOO-1 acts downstream of VAB-9 to stabilize junctional integrity.

That *zoo-1(RNAi);rrf-3* embryos rupture suggests reduced resistance of apical junctions to actomyosin-mediated contractility. We therefore generated hypocontractile *zoo-1(RNAi);rrf-3* embryos by using simultaneous weak RNAi against *let-502*/Rho kinase, and we enhanced contractility by performing *zoo-1(RNAi)* in *mel-11(it26)*/myosin phosphatase mutants, in which myosin presumably remains phosphorylated and hence abnormally active [18]. *let-502(RNAi)* resulted in a reduction of rupture of *zoo-1(RNAi);rrf-3* embryos from 12% to 4% (n = 66 and 116 embryos examined, respectively; significantly different, $p < 0.04$, Fisher's exact test), whereas *zoo-1(RNAi)* knockdown in *mel-1(it26)* homozygotes resulted in the appearance of early ruptures prior to the 1.5-fold stage (n = 53 and 22 embryos examined for *zoo-1(RNAi);mel-11(it26)* and *mel-11(it26)*, respectively; Figures 2M–2O; Figure S5; significantly different from *mel-11* alone, $p < 0.008$). Based on these results, we conclude that ZOO-1 is especially important to provide mechanical stability to epidermal junctions.

zoo-1 (RNAi) Reduces Junctional Actin Recruitment, Leading to Perturbed Actin Filaments

We next visualized actin dynamics with an F-actin reporter expressed specifically in the epidermis, the actin-binding domain of VAB-10 fused to GFP [19]. We observed a significant decrease in actin localized near cell-cell junctions. Actin in this region aligns into a robust cable parallel to cell-cell boundaries in *rrf-3* embryos (Figures 3A and 3C), whereas in *zoo-1(RNAi);rrf-3* embryos, junctional actin is less robust (Figures 3B and 3D). Quantitative analysis (see Figure S6 for description) confirms these observations: the ratio of junctional to cytoplasmic actin in wild-type is 2.16 ± 0.26 (mean ± SD, n = 22 cells in 4 embryos measured) versus 1.4 ± 0.2 in *zoo-1(RNAi);rrf-3* embryos (n = 23 cells in 5 embryos; significantly different based on a two-tailed Student's t test, $p < 0.01$). During elongation, actomyosin contractile forces act along circumferential actin bundles (CFBs), which attach at their ends to cell-cell junctions and are thought to distribute the forces driving elongation. In untreated embryos, CFBs are evenly spaced (Figure 3E). Strikingly, in *zoo-1 (RNAi)* embryos, some CFBs cluster abnormally

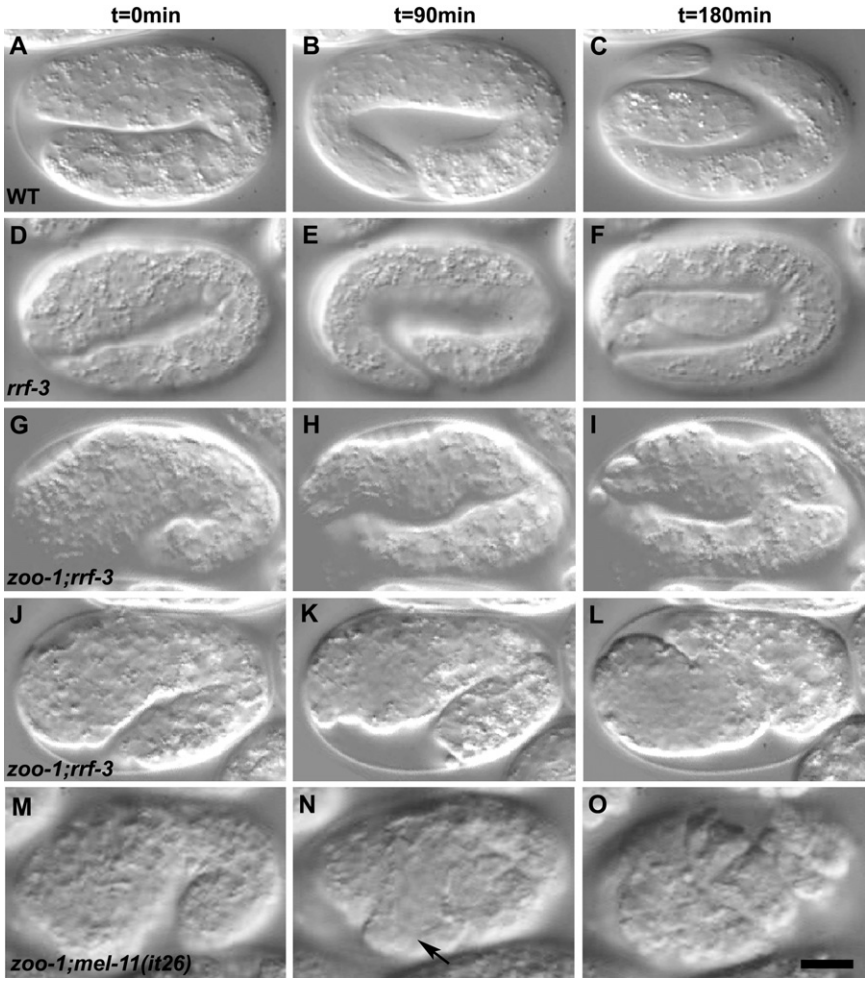

Figure 2. Loss of *zoo-1* Function Causes Embryonic Lethality

Nomarski images of representative embryos undergoing elongation are shown. t = 0 correlates with 90 min after ventral enclosure.

(A–C) Wild-type embryo.

(D–F) *rrf-3(pk1426)* embryo.

(G–I) *zoo-1(RNAi);rrf-3(pk1426)* embryo exhibiting failed elongation with pronounced body-shape defects.

(J–L) *zoo-1(RNAi);rrf-3(pk1426)* embryo that has ruptured from the posterior region. Note the delayed elongation of the *zoo-1(RNAi);rrf-3(pk1426)* embryos relative to wild-type.

(M–O) *zoo-1(RNAi);mel-11(it26)* embryo. Note the ventral rupture ([N], arrow).

Scale bar represents 10 μm.

(Figure 3F), suggesting that ZOO-1 contributes to their anchorage.

Because some *zoo-1(RNAi);rrf-3* embryos rupture during elongation, we imaged F-actin during ventral enclosure, when midline junctional connections are established. In contrast to wild-type embryos, which accumulate robust junctional actin at the ventral midline (Figure 3A; Movie S5), in *zoo-1(RNAi);rrf-3* embryos that display midline bulges near the end of enclosure, we consistently found loss of accumulation of midline junctional actin (Figure 3B; n = 6/6 embryos with midline defects examined), or failure to establish a midline connection entirely between one or more cells (Movies S6 and S7; n = 4/6 embryos with midline junctional failure). Taken together, the abnormalities in actin organization we observe in *zoo-1* knockdown embryos provide a mechanical explanation for observed defects at the end of ventral enclosure and during elongation.

zoo-1 (RNAi) Enhances the Lethality of *hmp-1*/α-Catenin and *hmp-2*/β-Catenin Hypomorphs

Connecting the actin cytoskeleton to cell-cell junctions is a role traditionally assigned to the cadherin-catenin complex [20]. Because ZOO-1 recruitment is independent of both α- and β-catenin, we hypothesized that ZOO-1 recruits actin to the junction in a parallel pathway. To test this hypothesis, we examined the combined effects of *zoo-1* (RNAi) and weak loss of function for β-catenin and α-catenin, by using *hmp-2* (*qm39*) ([21]; M. Costa, personal communication) and *hmp-1(fe4)* [22], respectively. *hmp-2(qm39)* displays 6% ± 1.2% (n = 832) embryonic and early larval lethality at 20°C (Table 1). In *hmp-2(qm39);zoo-1(RNAi)* embryos, lethality is significantly enhanced to 60% ± 4.6% (n = 508) and mutants exhibit delayed development (Table 1). Unlike wild-type embryos (Figure 4A), progeny of *hmp-1(fe4)* hermaphrodites show pronounced elongation defects (Figure 4B; Movie S8) and exhibit 77.5% ± 7.9% (n = 844) embryonic and early larval lethality (Table 1; [22]). Phalloidin staining of *hmp-1(fe4)* embryos confirms that the spatial arrangement of CFBs is occasionally perturbed ([27]; Figure 4E). *zoo-1(RNAi)* in *hmp-1(fe4)* mutants enhances overall lethality to 99.6% ± 1.8% (n = 818) and causes nearly all embryos to exhibit the Humpback phenotype (Figure 4D; Movie S9). Approximately half of *zoo-(RNAi);hmp-1(fe4)* mutants ultimately rupture at various positions along the body axis (Figure 4C; Movie S10).

zoo-1 loss of function also exacerbates the cytoskeletal defects observed in *hmp-1(fe4)* embryos: CFBs often cluster, resulting in inappropriately thick bundles (Figure 4F) similar to *hmp-1* null mutants and the most severe *hmp-1(fe4)* embryos [12, 22], suggesting that ZOO-1 and the cadherin complex act in parallel to stabilize actin at epidermal junctions. Loss of UNC-34/Ena also synergizes with *hmp-1(fe4)*, but unlike ZOO-1, UNC-34 is correctly localized in *hmr-1* mutant backgrounds [23]. We found no evidence for synergistic lethality between *zoo-1* and the null allele, *unc-34(gm104)* (data not shown).

In conclusion, we have provided in vivo analysis of ZOO-1/ZO-1 in *C. elegans*, and we show that ZOO-1 acts at junctions along with core AJ proteins during epithelial morphogenesis. Recent studies in *Drosophila* have implicated ZO-1/Pyd at AJs, based on defects in cell rearrangement during tracheal morphogenesis in *pyd* mutants [24]. However, these same studies have also implicated *pyd* in nuclear functions. Because it lacks the nuclear localization sequence found in other ZO-1 orthologs, ZOO-1 provides a "natural experiment" that can identify exclusively non-nuclear roles for ZO-1 proteins.

In ZO-1/ZO-2/ZO-3 knockdown cells in culture, AJ maturation is delayed [25]. In contrast, we do not find a delay in recruitment of core AJ components in *zoo-1* knockdown embryos in vivo. It is possible that the extremely rapid kinetics

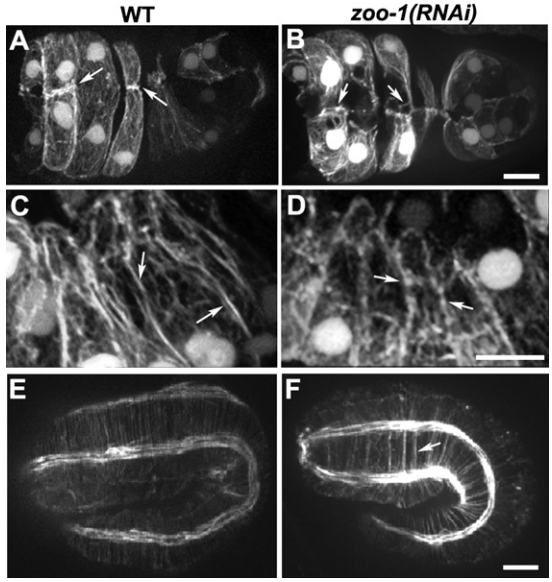

Figure 3. Loss of *zoo-1* Function Disrupts Actin Accumulation at Cell-Cell Junctions

(A and B) Ventral views of a wild-type (A) and *zoo-1(RNAi);rrf-3* (B) embryo at the end of ventral enclosure expressing a *gfp*-tagged fragment of *vab-10* that binds F-actin in epidermal cells [19]. In the wild-type embryo, two pairs of anterior cells have accumulated dense actin at the midline ([A], arrows), whereas only small actin puncta ([B], left arrow) or detached actin filaments ([B], right arrow) remain at the same position in the *zoo-1(RNAi);rrf-3* embryo ([B], arrows).

(C) Robust actin cables are visible at cell-cell borders in epidermal cells in a comma stage embryo (arrows).

(D) Actin is less evenly distributed at junctions in epidermal cells of comma stage *zoo-1* knockdown embryos (arrows).

(E and F) Embryos at the two-fold stage of elongation stained for F-actin.

(E) Wild-type embryo.

(F) *zoo-1(RNAi)* embryo. Note the abnormal clustering of circumferential actin filament bundles in the *zoo-1(RNAi)* embryo (arrow).

Scale bars represent 5 μm.

of junction formation in model invertebrates (minutes, as opposed to many hours in vertebrates) accounts for this difference, as has been previously suggested [22]. However, dynamic imaging of actin in living embryos after *zoo-1* knockdown revealed dramatic effects on actin recruitment at maturing junctions, which may be analogous to defects observed in the transition from "spot-like" to "belt-like" AJs in cultured cells after ZO protein depletion [25, 26]. Although ZO-1 directly binds actin [11, 27], the lack of sequence conservation in this region of ZOO-1 does not immediately suggest that ZOO-1 does so. Unfortunately, the dominant lethality of *zoo-1* transgenes has thus far precluded unambiguous structure-function analysis to address this issue.

C. elegans embryos undergoing epidermal morphogenesis do not require HMP-1/α-catenin or HMP-2/β-catenin for junctional recruitment of ZOO-1. In contrast, ZOO-1 recruitment does depend on HMR-1/E-cadherin and VAB-9/BCMP1. Because HMR-1 is required for proper junctional localization of VAB-9 [9], the simplest explanation for these localization results is HMR-1 → VAB-9 → → ZOO-1. Because there are very few cytoplasmic residues in VAB-9 that could engage in direct binding to ZOO-1, we think it unlikely that the interaction between the two proteins is direct. Instead, another protein presumably recruits ZOO-1 to AJs. Future studies that characterize the binding affinities of ZOO-1 at epidermal junctions should clarify the role of this highly conserved protein during morphogenesis.

Table 1. *zoo-1* Lethality in *rrf-3*, *hmp-1(fe4)*, and *hmp-2(qm39)*

Genotype	% Lethality	SD (n[a])
rrf-3(pk1426)	11.4	±6.3 (272)
zoo-1(RNAi);rrf-3(pk1426)	33.2	±5.9 (247)
hmp-1(fe4)	77.5	±7.9 (844)
zoo-1(RNAi);hmp-1(fe4)	99.6	±1.8 (818)
zoo-1(cxTi8317);hmp-1(fe4)	99.8	±0.6 (1114)
hmp-2(qm39)	6	±1.2 (832)
zoo-1(RNAi);hmp-2(qm39)	60	±4.6 (508)

[a] Number of embryos counted. Numbers are the sum of at least three separate experiments for each genotype.

Supplemental Data

Supplemental Data include Supplemental Results, Supplemental Experimental Procedures, six figures, and ten movies and can be found with this article online at http://www.current-biology.com/cgi/content/full/18/17/1333/DC1/.

Acknowledgments

We thank members of the Hardin lab for helpful discussion, Chris Lockwood for sharing unpublished data on *mel-11(it26)*, and M. Costa for sharing unpublished results regarding *hmp-2(qm39)*. Reagents were generously provided by Y. Kohara (cDNAs), L. Segalat (strain containing *zoo-1(cxTi8317)*), the International *C. elegans* Knockout Consortium (strain containing *zoo-1(gk404)*), and M. Labouesse (strain containing *vab-10::ABD::gfp*). Some *C. elegans* strains were obtained from the *C. elegans* Genetics Stock Center, which is funded by a grant from the NIH National Center for Research Support. This work was supported by NIH grant GM058038 to J.H. R.Z.-B. was supported by NIH postdoctoral training grant GM078747 and by a grant from the Machaiah Foundation.

Received: January 29, 2008
Revised: July 16, 2008
Accepted: July 17, 2008
Published online: August 21, 2008

References

1. Funke, L., Dakoji, S., and Bredt, D.S. (2005). Membrane-associated guanylate kinases regulate adhesion and plasticity at cell junctions. Annu. Rev. Biochem. *74*, 219–245.
2. Shin, K., Fogg, V.C., and Margolis, B. (2006). Tight junctions and cell polarity. Annu. Rev. Cell Dev. Biol. *22*, 207–235.
3. Yap, A.S., Crampton, M.S., and Hardin, J. (2007). Making and breaking contacts: The cellular biology of cadherin regulation. Curr. Opin. Cell Biol. *19*, 508–514.
4. Fesenko, I., Kurth, T., Sheth, B., Fleming, T.P., Citi, S., and Hausen, P. (2000). Tight junction biogenesis in the early *Xenopus* embryo. Mech. Dev. *96*, 51–65.
5. Rajasekaran, A.K., Hojo, M., Huima, T., and Rodriguez-Boulan, E. (1996). Catenins and zonula occludens-1 form a complex during early stages in the assembly of tight junctions. J. Cell Biol. *132*, 451–463.
6. Sheth, B., Fontaine, J.J., Ponza, E., McCallum, A., Page, A., Citi, S., Louvard, D., Zahraoui, A., and Fleming, T.P. (2000). Differentiation of the epithelial apical junctional complex during mouse preimplantation development: A role for rab13 in the early maturation of the tight junction. Mech. Dev. *97*, 93–104.
7. Yonemura, S., Itoh, M., Nagafuchi, A., and Tsukita, S. (1995). Cell-to-cell adherens junction formation and actin filament organization: Similarities and differences between non-polarized fibroblasts and polarized epithelial cells. J. Cell Sci. *108*, 127–142.
8. Cox, E.A., and Hardin, J. (2004). Sticky worms: Adhesion complexes in *C. elegans*. J. Cell Sci. *117*, 1885–1897.

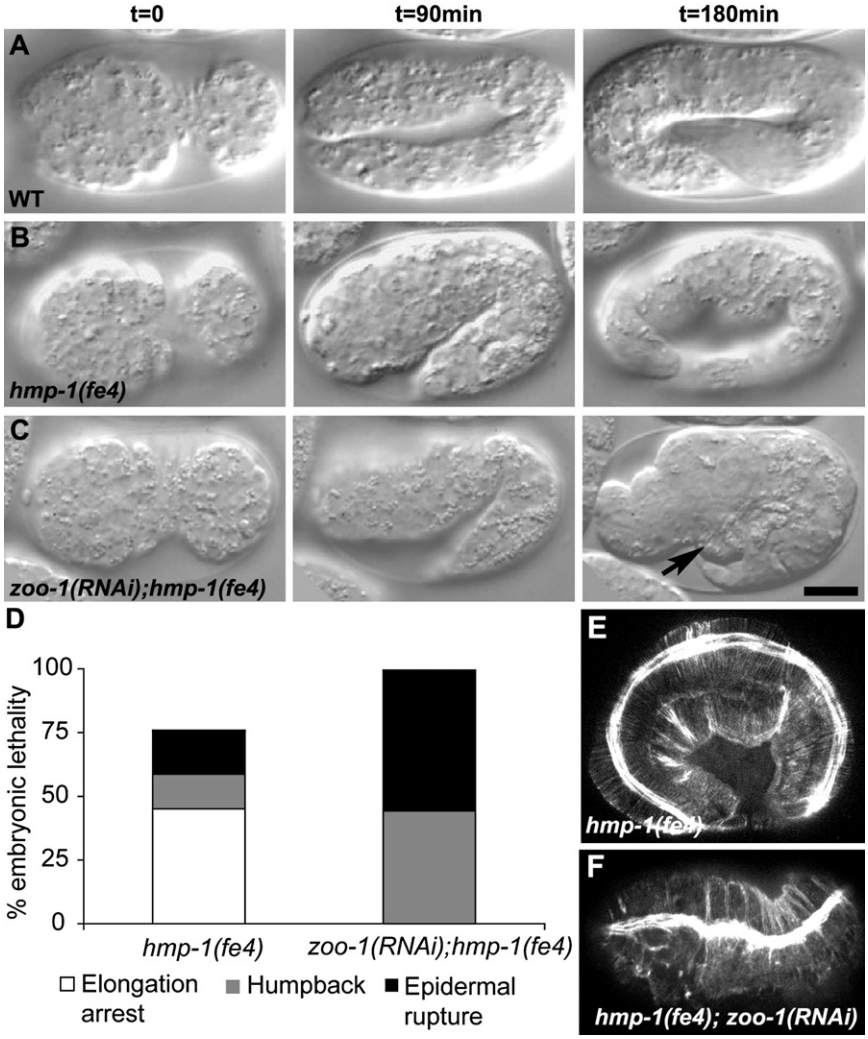

Figure 4. *zoo-1(RNAi)* Enhances the Elongation Defects of *hmp-1(fe4)* Mutants

(A–C) Nomarski images at 90 min time intervals of representative embryos undergoing elongation.
(A) Wild-type embryo.
(B) *hmp-1(fe4)* embryo with visible body-shape defects.
(C) *zoo-1(RNAi);hmp-1(fe4)* embryo that has ruptured from the ventral surface (arrow).
(D) Distribution of embryonic lethal phenotypes of *hmp-1(fe4)* and *zoo-1(RNAi);hmp-1(fe4)* animals.
(E and F) Representative confocal images of F-actin staining in a *hmp-1(fe4)* (E) and *zoo-1(RNAi);hmp-1(fe4)* (F) embryo. The organization of circumferential actin filaments is consistently and markedly disrupted in *zoo-1(RNAi);hmp-1(fe4)* embryos.
Scale bar represents 10 μm.

9. Simske, J.S., Köppen, M., Sims, P., Hodgkin, J., Yonkof, A., and Hardin, J. (2003). The cell junction protein VAB-9 regulates adhesion and epidermal morphology in *C. elegans*. Nat. Cell Biol. *5*, 619–625.
10. Imamura, Y., Itoh, M., Maeno, Y., Tsukita, S., and Nagafuchi, A. (1999). Functional domains of alpha-catenin required for the strong state of cadherin-based cell adhesion. J. Cell Biol. *144*, 1311–1322.
11. Itoh, M., Nagafuchi, A., Moroi, S., and Tsukita, S. (1997). Involvement of ZO-1 in cadherin-based cell adhesion through its direct binding to alpha catenin and actin filaments. J. Cell Biol. *138*, 181–192.
12. Costa, M., Raich, W., Agbunag, C., Leung, B., Hardin, J., and Priess, J.R. (1998). A putative catenin-cadherin system mediates morphogenesis of the *Caenorhabditis elegans* embryo. J. Cell Biol. *141*, 297–308.
13. Raich, W.B., Agbunag, C., and Hardin, J. (1999). Rapid epithelial-sheet sealing in the *Caenorhabditis elegans* embryo requires cadherin-dependent filopodial priming. Curr. Biol. *9*, 1139–1146.
14. Schneeberger, E.E., and Lynch, R.D. (2004). The tight junction: a multifunctional complex. Am. J. Physiol. Cell Physiol. *286*, C1213–C1228.
15. Miyoshi, J., and Takai, Y. (2005). Molecular perspective on tight-junction assembly and epithelial polarity. Adv. Drug Deliv. Rev. *57*, 815–855.
16. Asano, A., Asano, K., Sasaki, H., Furuse, M., and Tsukita, S. (2003). Claudins in *Caenorhabditis elegans*: Their distribution and barrier function in the epithelium. Curr. Biol. *13*, 1042–1046.
17. Simmer, F., Tijsterman, M., Parrish, S., Koushika, S.P., Nonet, M.L., Fire, A., Ahringer, J., and Plasterk, R.H. (2002). Loss of the putative RNA-directed RNA polymerase RRF-3 makes *C. elegans* hypersensitive to RNAi. Curr. Biol. *12*, 1317–1319.
18. Wissmann, A., Ingles, J., McGhee, J.D., and Mains, P.E. (1997). *Caenorhabditis elegans* LET-502 is related to Rho-binding kinases and human myotonic dystrophy kinase and interacts genetically with a homolog of the regulatory subunit of smooth muscle myosin phosphatase to affect cell shape. Genes Dev. *11*, 409–422.
19. Liegeois, S., Benedetto, A., Michaux, G., Belliard, G., and Labouesse, M. (2007). Genes required for osmoregulation and apical secretion in *Caenorhabditis elegans*. Genetics *175*, 709–724.
20. Weis, W.I., and Nelson, W.J. (2006). Re-solving the cadherin-catenin-actin conundrum. J. Biol. Chem. *281*, 35593–35597.
21. Hekimi, S., Boutis, P., and Lakowski, B. (1995). Viable maternal-effect mutations that affect the development of the nematode *Caenorhabditis elegans*. Genetics *141*, 1351–1364.
22. Pettitt, J., Cox, E.A., Broadbent, I.D., Flett, A., and Hardin, J. (2003). The *Caenorhabditis elegans* p120 catenin homologue, JAC-1, modulates cadherin-catenin function during epidermal morphogenesis. J. Cell Biol. *162*, 15–22.
23. Sheffield, M., Loveless, T., Hardin, J., and Pettitt, J. (2007). *C. elegans* Enabled exhibits novel interactions with N-WASP, Abl, and cell-cell junctions. Curr. Biol. *17*, 1791–1796.
24. Jung, A.C., Ribeiro, C., Michaut, L., Certa, U., and Affolter, M. (2006). Polychaetoid/ZO-1 is required for cell specification and rearrangement during *Drosophila* tracheal morphogenesis. Curr. Biol. *16*, 1224–1231.
25. Ikenouchi, J., Umeda, K., Tsukita, S., Furuse, M., and Tsukita, S. (2007). Requirement of ZO-1 for the formation of belt-like adherens junctions during epithelial cell polarization. J. Cell Biol. *176*, 779–786.
26. Yamazaki, Y., Umeda, K., Wada, M., Nada, S., Okada, M., and Tsukita, S. (2008). ZO-1/2-dependent integration of myosin-2 to epithelial zonula adherens. Mol. Biol. Cell, in press. Published online July 2, 2008. 10. 1091/mbc.E08-04-0352.
27. Fanning, A.S., Ma, T.Y., and Anderson, J.M. (2002). Isolation and functional characterization of the actin binding region in the tight junction protein ZO-1. FASEB J. *16*, 1835–1837.

Supplemental Data

The *C. elegans* Zonula Occludens Ortholog Cooperates with the Cadherin Complex to Recruit Actin during Morphogenesis

Christina Lockwood, Ronen Zaidel-Bar, and Jeff Hardin

Supplemental Results

Characterization of zoo-1 alleles

To examine consequences of loss of *zoo-1* function, we analyzed two *zoo-1* mutants, *gk404*, a 946-bp deletion of the first exon and surrounding promoter sequence, and *cxTi8317*, which contains a Tc5 transposon insertion predicted to disrupt the resulting GuK and Zu5 domains of ZOO-1 (Supplemental Figure 1). Neither allele confers a readily discernable phenotype; immunostaining reveals that ZOO-1 protein is produced in both backgrounds (data not shown). Although *zoo-1(gk404)* deletes exon 1 and the surrounding bases, we found that a message is indeed produced in *gk404* homozygotes that initiates from Met3 at the start of the second exon (data not shown). These data indicate that *gk404* and *cxTi8317* provide incomplete loss of *zoo-1* gene function.

Supplemental Experimental Procedures

C. elegans alleles and strains

Bristol N2 was used as the wild-type strain [1]. Nematodes were grown at 20°C in all experiments and were cultured as described [1]. *zoo-1(cxTi8317)* was kindly provided by L. Segalat [2]. All other strains were either constructed in our laboratory or obtained from the *Caenorhabditis* Genetics Center. The following mutations were used. LGI: *zoo-1(cxTi8317* and

gk404), hmp-2 (qm39) [3]. LGII: *rrf-3(pk1426)* [4], *vab-9(ju6)* [5]; *mel-11(it26)* [6]. LGV: *hmp-1(zu278* and *fe4)* [7, 8], *sma-1(e30)* [9], *daf-11(m84)* [9]. LGX: *dlg-1(ok318)*. Strain SU295 contains an integrated array (*jcIs24*) that includes *jac-1::gfp* and has not been mapped to a LG [8]. Strain SU292 contains an integrated *zoo-1::gfp* array (*jcIs22*) that has not been mapped to a LG.

Sequence analysis and identification of lesions in zoo-1 alleles

Protein sequence comparisons were performed using online tools available at the European Bioinformatics Institute (http://www.ebi.ac.uk/Tools/emboss/align/) and domain structure was analyzed using online tools available at Simple Modular Architecture Research Tool (SMART) (http://smart.embl-heidelberg.de/). We obtained the *zoo-1(gk404)* allele from the *C. elegans* Knockout Consortium and performed six outcrosses. We identified the lesion by isolating genomic DNA from homozygous hermaphrodites and amplified the genomic region with primers TT110 and TT111. The resulting amplification products were sequenced and confirmed that *gk404* contains a 946 bp deletion that removes all of exon 1 (96 bp) and 850 bp of the surrounding bases.

zoo-1(cxTi8317) was obtained from L. Segalat and was outcrossed six times and the insertion was molecularly tracked since animals homozygous for *cxTi8317* do not have an observable phenotype. Single hermaphrodites were allowed to lay progeny for 24 hours before their genomic DNA was isolated for analysis. The primer pair TT27 and TT74 flanks the insertion site and does not produce a product if the transposon is present and a 1.6 Kb product in wild-type worms. Primer set TT33 and Tc5.04 was also used for confirmation and amplified a 500 bp product only if the Tc5 transposon was present.

Construction of zoo-1::gfp transgene and transformation

A translational ZOO-1::GFP expression construct was created by ligating 5 Kb of genomic *zoo-1* sequence upstream of exon 2 to a 3.1 Kb *PstI* restriction fragment of *zoo-1* cDNA from yk621c6 (Y. Kohara). A second construct contained the *dlg-1* promoter [10] ligated to the *zoo-1* coding region. The fused products were cloned into the GFP vector, pPD95.75 (A. Fire). Standard microinjection techniques were used to create worms carrying the extrachromosomal array *jcEx81* [*zoo-1::gfp*, pRF4] and *jcEx70* [*Pdlg-1::zoo-1*, pRF4]. *jcIs22* was created by integrating *jcEx81* by gamma irradiation as described [5].

RT-PCR

RT-PCR was performed using Superscript III reagents (Invitrogen, Carlsbad, CA) as described [11]. Briefly, cDNA was synthesized from wild type and *zoo-1(gk404)* hermaphrodites using an oligo-d(T) primer for first-strand synthesis. Amplification of *zoo-1* or *act-1* (a positive control) cDNA was performed with gene-specific primers. Since EST data suggests that *zoo-1* can be alternatively spliced to remove exon 9, primer sets were designed that are capable of recognizing transcripts from either isoform.

RNAi

Two RNAi delivery methods were used to knockdown *zoo-1* maternal and zygotic product: injection and feeding. For injection, *zoo-1* cDNA was subcloned into two fragments encompassing the entire cDNA to facilitate efficient RNA transcription. Primer set TT26 and TT13 amplified a 1.6 Kb product that corresponds to the 5' region of *zoo-1*. We also amplified the 3' *zoo-1* cDNA region with primer sets TT27 and TT28, though subsequent experiments indicated that the 5' subclone alone is sufficient for ZOO-1 depletion (data not shown). RNA was transcribed *in vitro* according to the manufacturer's instructions (MegaScript T3 and T7 kits,

Ambion, Austin, TX). An ethanol ammonium acetate precipitation was used to recover RNA and product concentration was assessed by OD260 and confirmed by gel electrophoresis. Single-stranded RNA was diluted to an injection concentration of 2 μg/μl and sense/antisense annealing was carried out through incubation at 70°C for 10 minutes followed by incubation at 37°C for 30 minutes.

To construct a feeding clone, the 1.6 Kb *zoo-1* cDNA region that was successful for injection RNAi was subcloned into pPD129.36 using the *XbaI* and *HindIII* restriction sites and the resulting plasmid was transformed into HT115(DE3) bacteria. RNAi by feeding was performed essentially as described [12, 13].

cDNA clones obtained from Y. Kohara (Gene Network Lab, NIG, Japan) included: yk621c6 (*zoo-1*), yk36d4 (*hmp-1*), yk1047c6 (*hmp-2*), yk1230g8 (*hmr-1*), yk25e5 (*dlg-1*), yk304e5 (*clc-1*). RNA template for *clc-2* was produced by PCR amplification of genomic DNA using nested primers with the T3 or T7 promoter sequence added.

Permeability and contractility sensitivity assays

A dye tracer experiment was performed essentially as described [14]. In all observed animals, the pharynx/intestine was outlined without body cavity leakage. To test for sensitivity of *zoo-1(RNAi);rrf-3* embryos to changes in actomyosin contractility, we performed two experiments. To reduce *let-502* function, we performed feeding RNAi using *rrf-3* worms fed bacteria expressing either *zoo-1* and *let-502* dsRNA, or *zoo-1* dsRNA and an equivalent amount of L4440 bacteria. After 24 hr of feeding, worms were cut open, the embryos were extracted, and allowed to develop overnight on a watch glass. Embryos arrested during elongation were then counted. To examine effects of reducing *mel-11* activity, we performed *zoo-1* feeding RNAi on *mel-11(it26)* mutants, and

compared the results to *mel-11(it26)* alone. Embryos rupturing prior to 1.5-fold, after 1.5-fold, or exhibiting no rupture were scored from 4D movies. Statistical analyses were performed online using Fisher's 2 x 2 exact test or 2 x 3 test (http://www.quantitativeskills.com/sisa/statistics/fiveby2.htm).

Antibodies and embryo staining

For immunostaining, embryos were freeze cracked as described [7] and stained as described [5]. Embryos were fixed and prepared for staining with the following antibodies diluted in PBS with 1% BSA: affinity purified rabbit-α-ZOO-1 (Proteintech Group Inc., Chicago, IL; 1:500), monoclonal antibody (mAb) MH27 against AJM-1 ([15]; 1:50), mAb2085 against HMP-1 (Chemicon, Temecula, CA; 1:50). Double labeling with phalloidin and antibody was performed as described [8, 16].

Microscopy

4D Nomarski microscopy was performed as previously described [17]. Embryos were filmed on a Nikon Eclipse E600 or Optiphot-2 upright microscope equipped with DIC optics. NIH Image and ImageJ software were used to compress data into 4D QuickTime movies with custom macros/plugins (available at http://worms.zoology.wic.edu/4d/4d.html). Live imaging of GFP-expressing embryos was performed via spinning disc confocal microscopy with a Yokogawa CSU10 scanhead and a Hamamatsu ORCA-ER CCD camera. Fixed specimens were visualized using spinning disc confocal microscopy and collected with Perkin Elmer Ultraview software. In some figures, multiple focal planes were projected to generate images. For quantification of F-actin intensity, images were imported into and analyzed using the public domain program Priism [18], available at http://msg.ucsf.edu/IVE/index.html. For colocalization analysis, junctions from embryos immunostained for ZOO-1 and AJM-1, or stained for ZOO-1

and expressing JAC-1::GFP were 3d projected using ImageJ software. The resulting reconstructed junctional boundaries were manually traced and the relevant ROI was subjected to colocalization analysis using a plugin for ImageJ written by T. Collins, McMaster University (available at http://www.macbiophotonics.ca/imagej/installing_imagej.htm). Statistical analyses were performed using Microsoft Excel.

Supplemental References

1. Brenner, S. (1974). The genetics of Caenorhabditis elegans. Genetics *77*, 71-94.
2. Martin, E., Laloux, H., Couette, G., Alvarez, T., Bessou, C., Hauser, O., Sookhareea, S., Labouesse, M., and Segalat, L. (2002). Identification of 1088 new transposon insertions of Caenorhabditis elegans: a pilot study toward large-scale screens. Genetics *162*, 521-524.
3. Hekimi, S., Boutis, P., and Lakowski, B. (1995). Viable maternal-effect mutations that affect the development of the nematode Caenorhabditis elegans. Genetics *141*, 1351-1364.
4. Simmer, F., Tijsterman, M., Parrish, S., Koushika, S.P., Nonet, M.L., Fire, A., Ahringer, J., and Plasterk, R.H. (2002). Loss of the putative RNA-directed RNA polymerase RRF-3 makes C. elegans hypersensitive to RNAi. Curr Biol *12*, 1317-1319.
5. Simske, J.S., Koppen, M., Sims, P., Hodgkin, J., Yonkof, A., and Hardin, J. (2003). The cell junction protein VAB-9 regulates adhesion and epidermal morphology in C. elegans. Nat Cell Biol *5*, 619-625.
6. Wissmann, A., Ingles, J., McGhee, J.D., and Mains, P.E. (1997). Caenorhabditis elegans LET-502 is related to Rho-binding kinases and human myotonic dystrophy kinase and interacts genetically with a homolog of the regulatory subunit of smooth muscle myosin phosphatase to affect cell shape. Genes Dev *11*, 409-422.
7. Costa, M., Raich, W., Agbunag, C., Leung, B., Hardin, J., and Priess, J.R. (1998). A putative catenin-cadherin system mediates morphogenesis of the Caenorhabditis elegans embryo. J Cell Biol *141*, 297-308.
8. Pettitt, J., Cox, E.A., Broadbent, I.D., Flett, A., and Hardin, J. (2003). The Caenorhabditis elegans p120 catenin homologue, JAC-1, modulates cadherin-catenin function during epidermal morphogenesis. J Cell Biol *162*, 15-22.
9. McKeown, C., Praitis, V., and Austin, J. (1998). sma-1 encodes a betaH-spectrin homolog required for Caenorhabditis elegans morphogenesis. Development *125*, 2087-2098.
10. Lockwood, C.A., Lynch, A.M., and Hardin, J. (2008). Dynamic analysis identifies novel roles for DLG-1 subdomains in AJM-1 recruitment and LET-413-dependent apical focusing. J Cell Sci *121*, 1477-1487.

11. Thomas-Virnig, C.L., Sims, P.A., Simske, J.S., and Hardin, J. (2004). The inositol 1,4,5-trisphosphate receptor regulates epidermal cell migration in Caenorhabditis elegans. Curr Biol *14*, 1882-1887.
12. Kamath, R.S., Fraser, A.G., Dong, Y., Poulin, G., Durbin, R., Gotta, M., Kanapin, A., Le Bot, N., Moreno, S., Sohrmann, M., et al. (2003). Systematic functional analysis of the Caenorhabditis elegans genome using RNAi. Nature *421*, 231-237.
13. Timmons, L. (2006). Delivery methods for RNA interference in C. elegans. Methods Mol Biol *351*, 119-125.
14. Asano, A., Asano, K., Sasaki, H., Furuse, M., and Tsukita, S. (2003). Claudins in Caenorhabditis elegans: their distribution and barrier function in the epithelium. Curr Biol *13*, 1042-1046.
15. Koppen, M., Simske, J.S., Sims, P.A., Firestein, B.L., Hall, D.H., Radice, A.D., Rongo, C., and Hardin, J.D. (2001). Cooperative regulation of AJM-1 controls junctional integrity in Caenorhabditis elegans epithelia. Nat Cell Biol *3*, 983-991.
16. Costa, M., Draper, B.W., and Priess, J.R. (1997). The role of actin filaments in patterning the Caenorhabditis elegans cuticle. Dev Biol *184*, 373-384.
17. Raich, W.B., Agbunag, C., and Hardin, J. (1999). Rapid epithelial-sheet sealing in the Caenorhabditis elegans embryo requires cadherin-dependent filopodial priming. Curr Biol *9*, 1139-1146.
18. Chen, H., Clyborne, W., Sedat, J.W., and Agard, D.A. (1992). PRIISM: an integrated system for display and analysis of three-dimensional microscope images. Proc. of SPIE *1660*, 784-790.

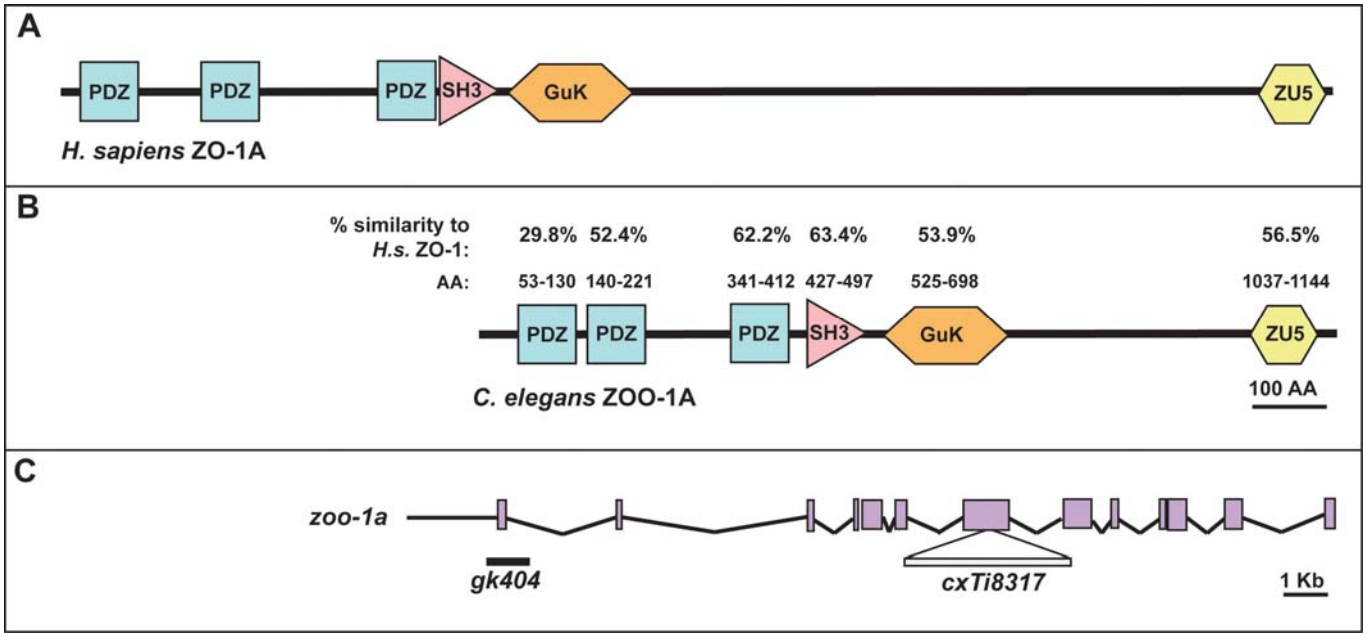

Figure S1. *zoo-1* encodes a *C. elegans* Zonula Occludens Ortholog.

Although the overall amino acid similarity of ZOO-1A to *Homo sapiens* ZO-1A is 34.2%, individual domains show much higher conservation. (A) Schematic structure of *H. sapiens* ZO-1A, which contains the following domains: PDZ, PSD-95, Dlg-1, ZO-1; SH3, Src Homology 3; GuK, Guanylate Kinase; ZU5, ZO-1, UNC-5 proline-rich region. (B) Schematic structure of ZOO-1. Amino acid residues of ZOO-1A corresponding to each region based on SMART predictions are indicated, as is the percent amino acid similarity within each domain compared to *H. sapiens* ZO-1A. (C) Structure of the *zoo-1* gene is shown with exons represented by boxes. Alleles *gk404* and *cxTi8317* are indicated.

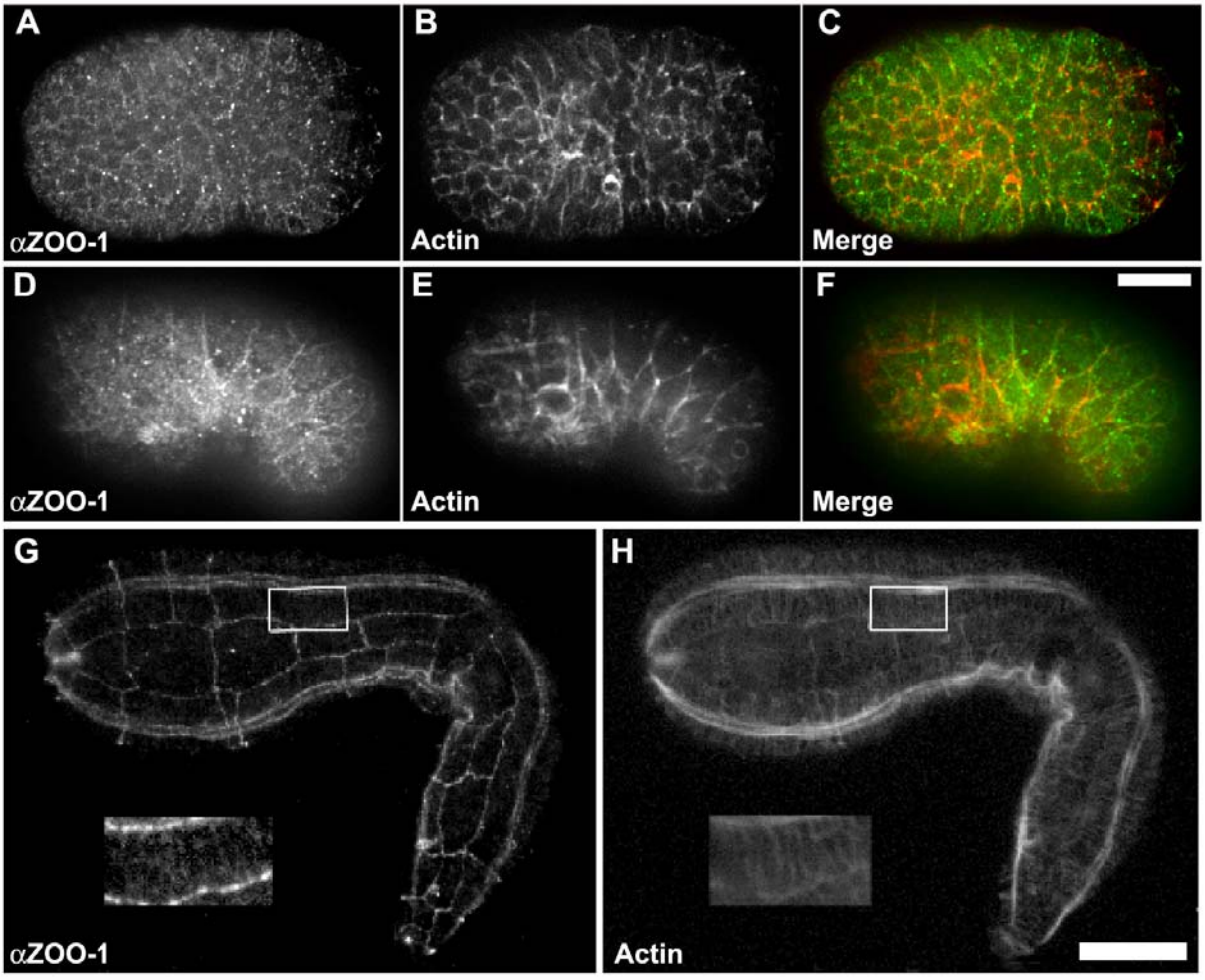

Figure S2. ZOO-1 colocalizes with actin at cell borders during morphogenesis.

Confocal images of embryos stained for ZOO-1 (A,D,G), F-actin (B,E,H), and the merge (C,F). (A-C) Embryo beginning ventral enclosure. (D-F) Embryo at the 1.25-stage of elongation has increased ZOO-1 at cell borders. (G, H) Embryo at the 2-fold stage of elongation has robust junctional ZOO-1. Insets in G and H are enlargements of the boxed regions. Scale bar, 10 μm.

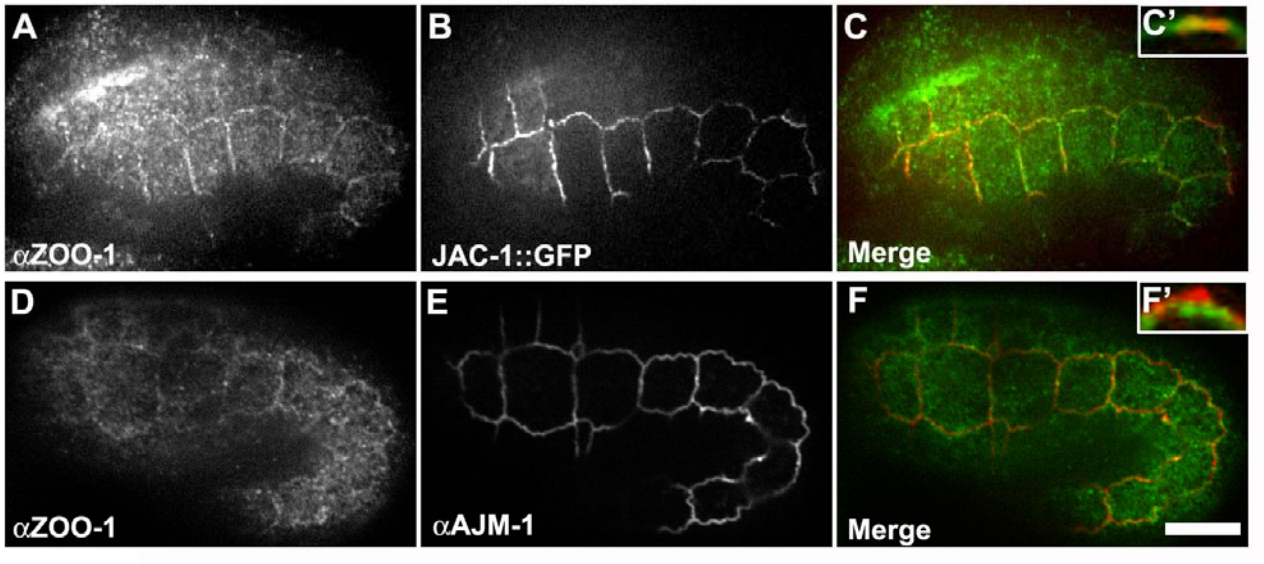

Figure S3. ZOO-1 colocalizes with the cadherin complex in the epidermis.

(A-C) Confocal images showing a comma stage embryo stained for ZOO-1 (A) that is also expressing JAC-1/p120-catenin::GFP (B). The merged image is shown in C (ZOO-1, red; JAC-1, green). C' shows a projected region of a junction in sagittal profile enlarged 3X. (D-F) Confocal images of a 1.5-fold stage embryo stained for ZOO-1 (D) and AJM-1 (E). The merged image is shown in F (ZOO-1, red; AJM-1, green). F' shows a projected region of a junction in sagittal profile enlarged 3X. Scale bar, 10 μm. Quantitative colocalization analysis confirms that ZOO-1 colocalizes with the cadherin complex. For JAC-1, $r^2 = 0.72 \pm 0.05$, mean ± SEM, n = 3, whereas for AJM-1, $r^2 = 0.39 \pm 0.05$, n = 3 (significantly different from JAC-1, $p < 0.004$, Fisher's exact test).

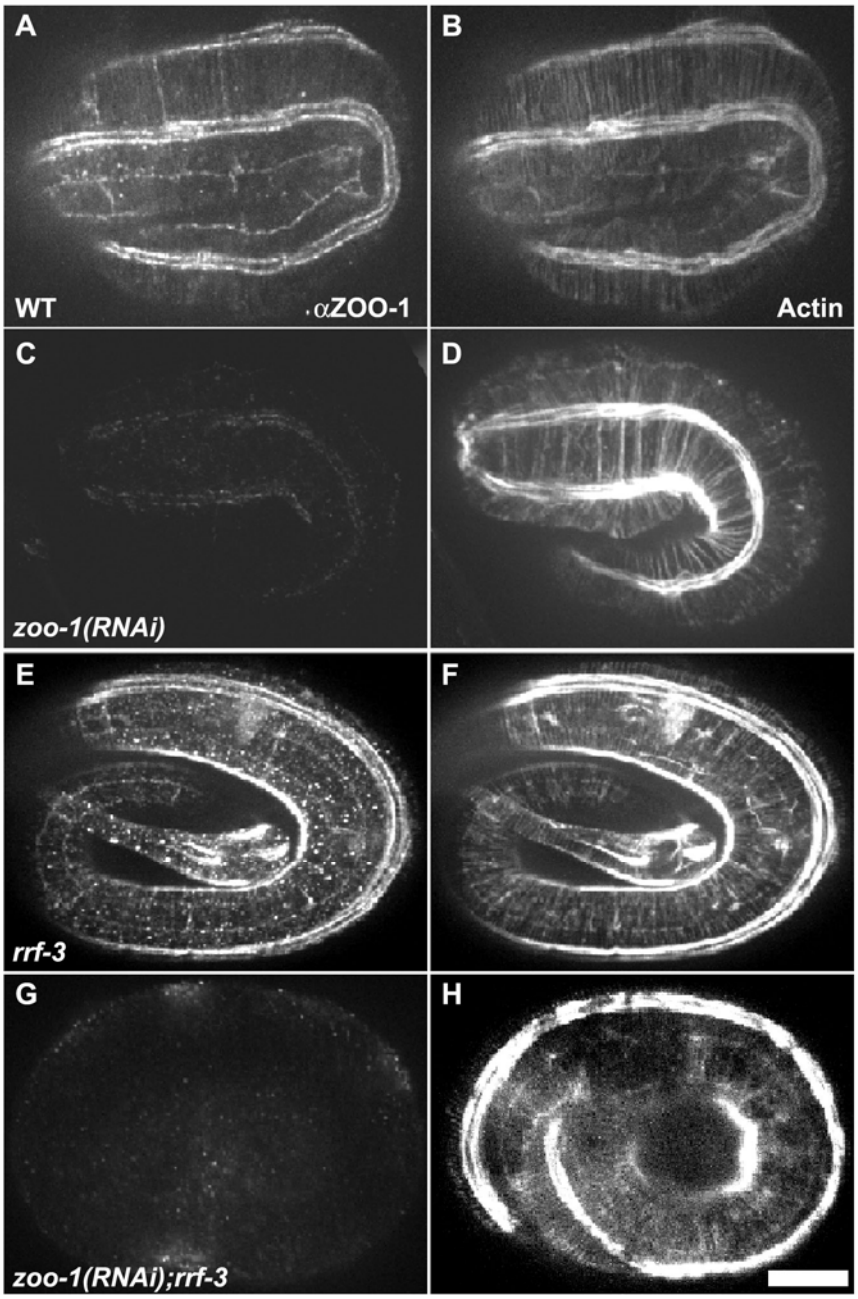

Figure S4. *zoo-1(RNAi);rrf-3(pk1426)* gene knockdown abolishes antibody signal. Embryos are stained for ZOO-1 (left column) and F-actin (right column). (A, B) Wild-type two-fold embryo corresponding to Figure 3E. (C, D) Two-fold *zoo-1(RNAi)* embryo, corresponding to Figure 3F. (E, F) Three-fold *rrf-3(pk1426)* embryo. (G, H) Three-fold *zoo-1(RNAi);rrf-*

3(pk1426) embryo. Compare residual levels of ZOO-1 in a *zoo-1(RNAi)* background (C) versus complete absence of ZOO-1 in *zoo-1(RNAi);rrf-3(pk1426)* (G). Scale bar, 10 μm.

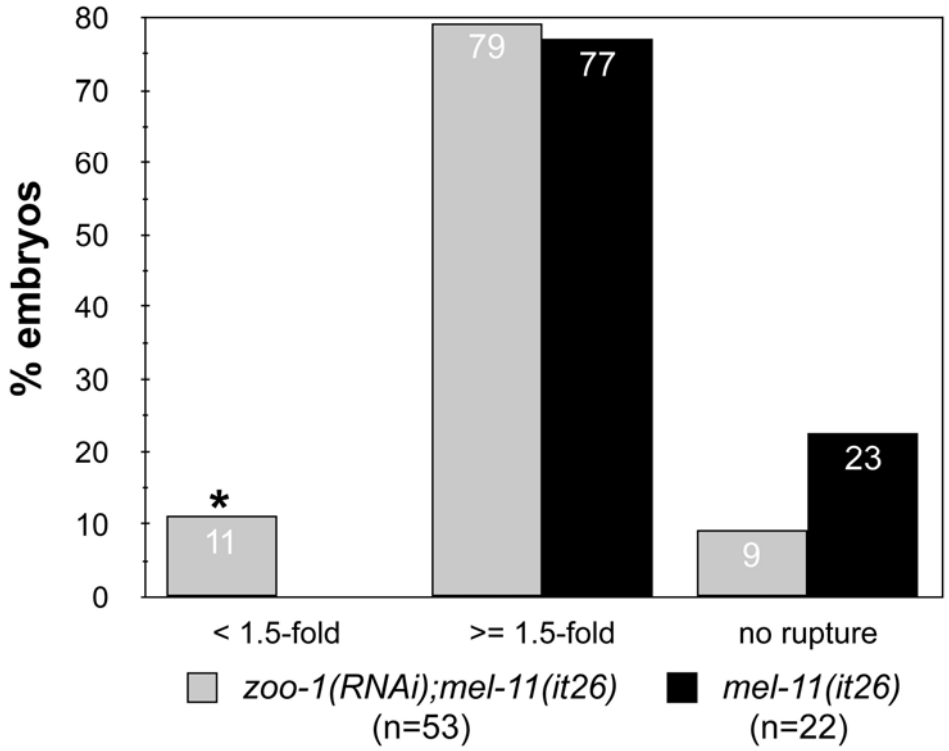

Figure S5. Loss of *zoo-1* function enhances rupture defects in *mel-11(it26)* hypercontractile mutants.

The percentage arrested at various stages of elongation was scored for *zoo-1(RNAi); mel-11(it26)* and *mel-11(it26)* embryos. Asterisk: significantly different, $p < 0.001$ (Fisher's exact test).

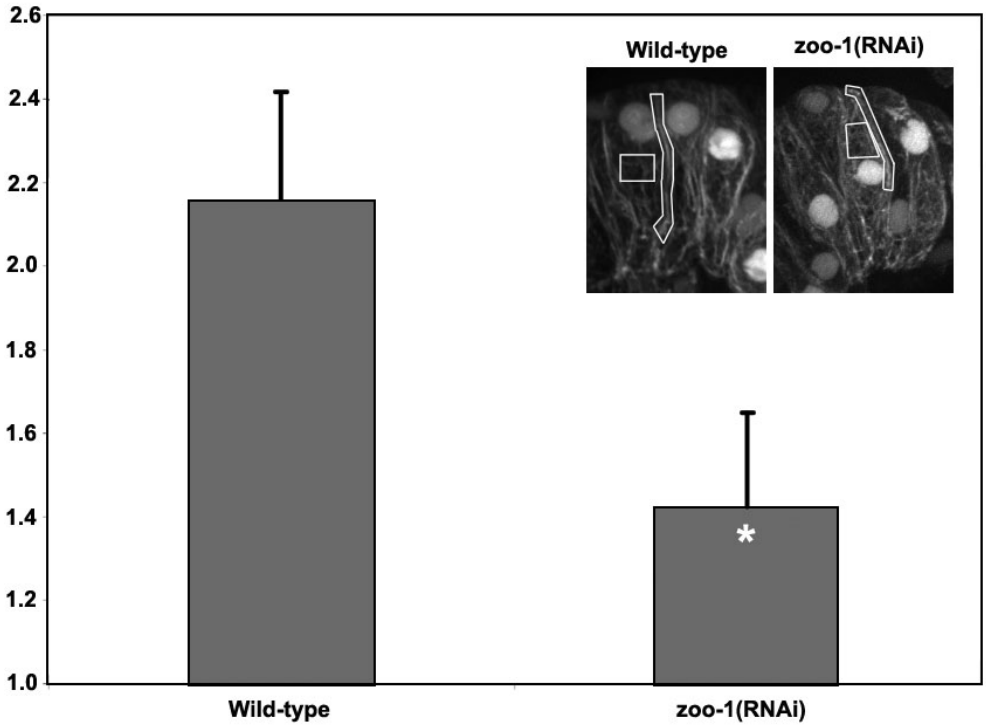

Figure S6. *zoo-1(RNAi);rrf-3* embryos accumulate less actin at cell borders.

The ratio of junctional to cytoplasmic actin was measured as described in Materials and Methods. Sample ROIs for representative wild-type and *zoo-1(RNAi);rrf-3* embryos are shown (inset). Asterisk: significantly different, $p < 0.01$(two-tailed student t-test).